



Hall device impacts on ciliated pump-assisted blood flow of double-diffusion convection of nanofluid in a porous divergent channel

Ying-Qing Song¹, Khurram Javid², Sami Ullah Khan³, M. Ijaz Khan⁴,
Tian-Chuan Sun^{5,a}, M. Imran Khan^{6,b}, M. Y. Malik⁷

¹ School of Science, Hunan City University, Yiyang 413000, People's Republic of China

² Department of Mathematics, Northern University, Wattar-Wallai Road, Nowshera 24110, KPK, Pakistan

³ Department of Mathematics, COMSATS University Islamabad, Sahiwal 57000, Pakistan

⁴ Department of Mathematics and Statistics, Riphah International University, I-14, Islamabad 44000, Pakistan

⁵ Qiuzhen College, Huzhou University, Huzhou 313000, People's Republic of China

⁶ CECOS University of IT and Emerging Sciences, Peshawar, Pakistan

⁷ Department of Mathematics, College of Sciences, King Khalid University, Abha 61413, Kingdom of Saudi Arabia

Received: 26 April 2021 / Accepted: 4 June 2021

© The Author(s), under exclusive licence to Società Italiana di Fisica and Springer-Verlag GmbH Germany, part of Springer Nature 2021

Abstract Motivated by bio-chemical systems and ciliated propulsion, we consider the steady laminar flow from a non-uniform wavy channel adjacent to a saturated porous medium which has been investigated analytically using an integration technique. A highly permeability domain is considered. We employed a sinusoidal complex wavy relation for the ciliated walls. A mathematical relation was used to convert the rheological equations from $(\bar{X}, \bar{\xi})$ coordinate system to a $(\bar{x}, \bar{\xi})$ dimensionless system. These rheological equations are simplified under two biological assumptions, one is creeping phenomena, and the second one is long-wavelength approximation. The solution of governing equations is obtained through Mathematica software 10.0 with the help of integration technique in a wave frame. The impacts of embedded hydro-mechanical parameters on the rheological features are studied. The boundary layer phenomena are obtained in the velocity profile under larger magnetic and porosity effects. The magnitude of pressure gradient is reduced under larger strength of magnetic and porosity effects. The cilia length parameter has a dynamic role in enhancement of the pressure gradient. The larger strength of the thermophoretic parameter has remarkable effects in augmentation of volumetric fraction, heat and mass transfer phenomena. The outcomes of current investigation are applicable in energy systems, manufacturing of ciliated micro-pumps, petroleum engineering, thermal augmentation of physiological and chemical fluids, and industrial magnetic materials processing.

^a e-mail: suntch@zjhu.edu.cn (corresponding author)

^b e-mail: mk42@hw.ac.uk (corresponding author)

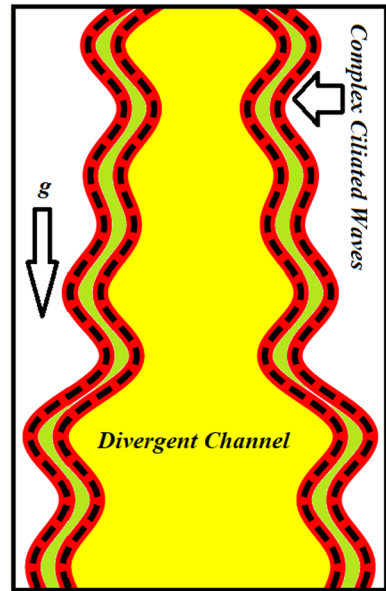
1 Introduction

Cilia is microscopic fur-like configurations that exist in almost every living cell of human bodies. Cilia is highly conserved organisms that oblige sensory functions, motile functions and sometimes both. These organisms have the ability to deform in a wavelike structure to push cells and to produce fluid streams in numerous organs of the living body. The metachronal wave is a sequential action of cilia beating that refers to wavy movements. Due to their particular metachronism, cilia play a dynamic role in some biological cycles such as respiration, reproduction, circulation, locomotion and alimentation [1–7]. According to the dynamic study mentioned in citations [8, 9], any deform in the cilia transportation can cause some anthropological syndromes. All these theoretical studies mentioned above give productive information about the motion of biological fluids that surround them; it is valuable and helpful to apprehend different biological frameworks in the human body.

After these magnificent contributions, lots of mathematicians performed vital contributions in this direction and attempted dynamic contributions in this domain. These are cited in the following references [10–14]. In 2014, Siddiqui et al., [10] investigated a mathematical formulation of a viscous fluid flow through a cylindrical tube due to ciliary beating under magnetic effects. They noticed that the pumping phenomena are more productive under the larger strength of the magnetic effect. In another study, Siddiqui et al., [11] performed an analytical study of cilia motion of viscous fluid in a channel. Their whole analysis is based on creeping phenomena. They observed that under larger magnetic effects, the circulation of bolus in trapping phenomena is reduced. They also compared their results with the flow rate of spermatic fluid through the ductus efferentes. Farooq et al. [12] studied the fully developed flow of viscous fluid in a vertical channel under biological approximation of lubrication theory in a wave frame. They also observed the impacts of the magnetic field on flow features. They found the analytical solutions of rheological equations by using adomian decomposition method. The cilia propulsion of viscous fluid through a curved channel was studied by Asghar et al., [13]. Their whole analysis is based on a complex wavy pattern of metachronal waves and physical effects of porosity parameter. They used curvilinear coordinates in the derivation of rheological equations and solved these equations analytically with the help of integration technique. Javid et al., [14] studied the motion of biological fluid in non-uniform geometry under combined effects of magnetic and electric field. The flow equations are solved numerically by using the BVP4C technique. They noticed that non-uniform parameters and cilia length have a vital role in transportation of biological fluid.

From the past two decades, nanofluids have gained significant courtesy in chemical and engineering domains. Nanofluid is a fluid that contains nanoparticles and the diameter of these particles is less than 100 nm. These nanoparticles are comprised of metals, for example, aluminum oxides, copper oxides, nitrides or nano-metals. Choi [15] experimentally confirmed that involvement of nano-size particles into the base liquid outcomes in the appreciable augmentation in thermo-physical features of the base liquid. After the remarkable contribution of Choi [15], researchers have utilized this idea of nanofluid in order to boost the performance of heat transfer phenomena in numerous liquids. Therefore, various review articles [16–20] including the advancement of nanofluid performance have been reported over the most recent couple of years, mainly focused on analytical and numerical investigations of the thermo-physical properties or the convective heat transfer of nanofluids. Kuznetsov and Nield [21] studied the boundary layer flow of nanofluid in a vertical plate along with natural convection. After one year of their study, they expanded their mathematical study for double-diffusion convection [22]. A few investigations [23–28] on single and double diffusion convection in nanofluids is numerous nature of flow channels have been introduced.

Fig. 1 Geometry of the porous-divergent channel



In the present investigation, the ciliated transport of nanofluid through a non-uniform channel under biological approximations is presented. Furthermore, the impact of the Hall device and porous medium on the cilia propulsion of nanofluid along with double diffusion convection is discussed. The complex wavy scenario is taken in both boundary walls in order to enhance the efficiency of ciliated micro-pumps. The physical impacts of involved physical variables on the velocity profile, ciliated-pumping, trapping, volumetric fraction, heat and mass transfer phenomena are investigated analytically and illustrated graphically.

2 Nanofluid mathematical modeling

2.1 Non-Uniform flow geometry

In the present flow analysis, the ciliated transportation of two-dimensional nanofluid is considered through a non-uniform flow geometry. Initially, the fluid is at rest, and its motion takes place because of the metachronal waves present at the walls of the flow regime. The complex nature of metachronal waves is considered in the current study in order to boost the performance of non-uniform ciliated-pumps. Furthermore, the double-diffusion convection is also considered in the nanofluid flow analysis. The flow geometry under the discussion is displayed in Fig. 1.

The constitutive equation for the complex flow geometry is mathematically defined by:

$$\begin{aligned} \bar{H}(\bar{X}, \bar{t}) = Cl \left(\bar{C}_1 \sin \left(\frac{\bar{\beta}_1}{\omega} (\bar{X} - s\bar{t}) \right) + \bar{C}_2 \sin \left(\frac{\bar{\beta}_2}{\omega} (\bar{X} - s\bar{t}) \right) + \bar{C}_3 \sin \left(\frac{\bar{\beta}_3}{\omega} (\bar{X} - s\bar{t}) \right) \right) \\ + b + \bar{\alpha}(\bar{X} - s\bar{t}) = \bar{G}(\bar{X}, \bar{t}), \quad (\text{Upper Ciliated Wall}) \end{aligned} \tag{1}$$

$$\begin{aligned}
 -\bar{H}(\bar{X}, \bar{t}) = & -Cl \left(\bar{C}_1 \sin\left(\frac{\bar{\beta}_1}{\omega}(\bar{X} - s\bar{t})\right) + \bar{C}_2 \sin\left(\frac{\bar{\beta}_2}{\omega}(\bar{X} - s\bar{t})\right) + \bar{C}_3 \sin\left(\frac{\bar{\beta}_3}{\omega}(\bar{X} - s\bar{t})\right) \right) \\
 & - b - \bar{\alpha}(\bar{X} - s\bar{t}) = -\bar{G}(\bar{X}, \bar{t}), \quad (\text{Lower Ciliated Wall}) \tag{2}
 \end{aligned}$$

In the above equations, \bar{X} is the axial coordinate, $\bar{\xi}$ is the tangential coordinate, \bar{t} is the time, ω is the wavelength, b is the channel half width, Cl is the cilia length parameter with respect to amplitudes, $\bar{\alpha}$ is the non-uniform parameter, \bar{C}_k ($k = 1 - 3$) are the wave amplitudes, ω is the wavelength, s is the wave speed, and $\bar{\beta}_i$ ($i = 1 - 3$) are the physical parameters. Equations (1) and (2) must satisfy the physical property that is define as: $b \leq \bar{\beta}_1 + \bar{\beta}_2 + \bar{\beta}_3$. Let us consider, \bar{W} is the axial component of velocity and \bar{U} is the *transverse* component of velocity. There is no flow in the orthogonal plane (z -direction).

The mathematical form of cilia tips in the axial direction is defined as:

$$\begin{aligned}
 \bar{X} = \bar{X}_0 + Cl\kappa \left\{ \bar{C}_1 \sin\left(\frac{\bar{\beta}_1}{\omega}(\bar{X} - s\bar{t})\right) + \bar{C}_2 \sin\left(\frac{\bar{\beta}_2}{\omega}(\bar{X} - s\bar{t})\right) + \bar{C}_3 \sin\left(\frac{\bar{\beta}_3}{\omega}(\bar{X} - s\bar{t})\right) \right\} \\
 = \bar{F}(\bar{X}, \bar{X}_0, \bar{t}), \tag{3}
 \end{aligned}$$

where κ is the eccentricity of the elliptical motion and \bar{X}_0 is the reference position of the particle.

The rheological equations describing the unsteady transportation of two-dimensional nano-fluid along with double diffusion convection through the non-uniform ciliated micro-pump under some external forces, such as magnetic force, porosity medium and Hall devices, can be stated in terms Cartesian coordinate system $(\bar{X}, \bar{\xi})$ as follows:

$$\frac{\partial \bar{U}}{\partial \bar{X}} + \frac{\partial \bar{W}}{\partial \bar{\xi}} = 0, \tag{4}$$

$$\begin{aligned}
 \rho \left(\frac{\partial \bar{U}}{\partial \bar{t}} + \bar{U} \frac{\partial \bar{U}}{\partial \bar{X}} + \bar{W} \frac{\partial \bar{U}}{\partial \bar{\xi}} \right) = & - \frac{\partial \bar{P}}{\partial \bar{X}} + \mu \left(\frac{\partial^2 \bar{U}}{\partial \bar{X}^2} + \frac{\partial^2 \bar{U}}{\partial \bar{\xi}^2} \right) \\
 & + G \left\{ (1 - \Omega') \rho' (a_t (\bar{T} - T') + a_c (\bar{C} - C')) - (\rho_p - \rho') (\bar{\Omega} - \Omega') \right\} \\
 & - \frac{\mu}{K} \bar{U} - \frac{\sigma' B_0^2}{1 + M^2} \bar{U}, \tag{5}
 \end{aligned}$$

$$\begin{aligned}
 \rho \left(\frac{\partial \bar{W}}{\partial \bar{t}} + \bar{U} \frac{\partial \bar{W}}{\partial \bar{X}} + \bar{W} \frac{\partial \bar{W}}{\partial \bar{\xi}} \right) = & - \frac{\partial \bar{P}}{\partial \bar{\xi}} + \mu \left(\frac{\partial^2 \bar{W}}{\partial \bar{X}^2} + \frac{\partial^2 \bar{W}}{\partial \bar{\xi}^2} \right) \\
 & + G \left\{ (1 - \Omega') \rho' (a_t (\bar{T} - T') + a_c (\bar{C} - C')) - (\rho_p - \rho') (\bar{\Omega} - \Omega') \right\} \\
 & - \frac{\mu}{K} \bar{W} - \frac{\sigma' B_0^2}{1 + M^2} \bar{W}, \tag{6}
 \end{aligned}$$

$$\begin{aligned}
 (\rho c_p) \left(\frac{\partial \bar{T}}{\partial \bar{t}} + \bar{U} \frac{\partial \bar{T}}{\partial \bar{X}} + \bar{W} \frac{\partial \bar{T}}{\partial \bar{\xi}} \right) = & k' \left(\frac{\partial^2 \bar{T}}{\partial \bar{X}^2} + \frac{\partial^2 \bar{T}}{\partial \bar{\xi}^2} \right) + dtc \left(\frac{\partial^2 \bar{C}}{\partial \bar{X}^2} + \frac{\partial^2 \bar{C}}{\partial \bar{\xi}^2} \right) \\
 & + \left\{ db \left(\frac{\partial \bar{\Omega}}{\partial \bar{X}} \frac{\partial \bar{T}}{\partial \bar{X}} + \frac{\partial \bar{\Omega}}{\partial \bar{\xi}} \frac{\partial \bar{T}}{\partial \bar{\xi}} \right) + \frac{dt}{T_0} \left(\left(\frac{\partial \bar{T}}{\partial \bar{X}} \right)^2 + \left(\frac{\partial \bar{T}}{\partial \bar{\xi}} \right)^2 \right) \right\}, \tag{7}
 \end{aligned}$$

$$\left(\frac{\partial \bar{C}}{\partial \bar{t}} + \bar{U} \frac{\partial \bar{C}}{\partial \bar{X}} + \bar{W} \frac{\partial \bar{C}}{\partial \bar{\xi}} \right) = ds \left(\frac{\partial^2 \bar{C}}{\partial \bar{X}^2} + \frac{\partial^2 \bar{C}}{\partial \bar{\xi}^2} \right) + dct \left(\frac{\partial^2 \bar{T}}{\partial \bar{X}^2} + \frac{\partial^2 \bar{T}}{\partial \bar{\xi}^2} \right), \tag{8}$$

$$\left(\frac{\partial \bar{\Omega}}{\partial \bar{t}} + \bar{U} \frac{\partial \bar{\Omega}}{\partial \bar{X}} + \bar{W} \frac{\partial \bar{\Omega}}{\partial \bar{\xi}} \right) = db \left(\frac{\partial^2 \bar{\Omega}}{\partial \bar{X}^2} + \frac{\partial^2 \bar{\Omega}}{\partial \bar{\xi}^2} \right) + \frac{dt}{\tau_0} \left(\frac{\partial^2 \bar{T}}{\partial \bar{X}^2} + \frac{\partial^2 \bar{T}}{\partial \bar{\xi}^2} \right), \tag{9}$$

where ρ is the density, ρ_p is the density of nanoparticle mass, ρ' is the density of nanofluid at T' , \bar{P} is the pressure, \bar{T} is the temperature, \bar{C} is the concentration, $\bar{\Omega}$ is the volume fraction, g is the gravity, μ is the dynamic viscosity, K is the permeability of surface, d_{tc} is the thermal diffusivity, d_{ct} is the Soret diffusivity, d_s is the solutal diffusivity, σ is the electrical conductivity, db is the Brownian diffusion coefficient, dt is the thermophoretic diffusion coefficient, k' is the thermal conductivity, a_v is the volumetric thermal coefficient, a_c is the volumetric concentration coefficient, (ρc_p) is the heat capacities, B_0 is the dimensional magnetic parameter and M is the dimensional Hall parameter.

The transverse component of velocity is

$$\bar{U} = \left. \frac{\partial \bar{G}}{\partial \bar{t}} \right|_{\bar{x}_0} = \frac{\partial \bar{G}}{\partial \bar{t}} + \frac{\partial \bar{G}}{\partial \bar{X}} \frac{\partial \bar{G}}{\partial \bar{t}} = \frac{\partial \bar{G}}{\partial \bar{t}} + \frac{\partial \bar{G}}{\partial \bar{X}} \bar{U}. \tag{11}$$

After using Eq. (1), Eq. (11) reduces to

$$\bar{U} = \frac{-s\bar{\alpha} - \frac{Cl_s}{\omega} \left\{ \bar{\beta}_1 \bar{\epsilon}_1 \cos\left(\frac{\bar{\beta}_1}{\omega}(\bar{X} - s\bar{t})\right) + \bar{\beta}_2 \bar{\epsilon}_2 \cos\left(\frac{\bar{\beta}_2}{\omega}(\bar{X} - s\bar{t})\right) + \bar{\beta}_3 \bar{\epsilon}_3 \cos\left(\frac{\bar{\beta}_3}{\omega}(\bar{X} - s\bar{t})\right) \right\}}{1 - \bar{\alpha} - \frac{Cl}{\omega} \left\{ \bar{\beta}_1 \bar{\epsilon}_1 \cos\left(\frac{\bar{\beta}_1}{\omega}(\bar{X} - s\bar{t})\right) + \bar{\beta}_2 \bar{\epsilon}_2 \cos\left(\frac{\bar{\beta}_2}{\omega}(\bar{X} - s\bar{t})\right) + \bar{\beta}_3 \bar{\epsilon}_3 \cos\left(\frac{\bar{\beta}_3}{\omega}(\bar{X} - s\bar{t})\right) \right\}}. \tag{12}$$

The axial component of velocity is

$$\bar{W} = \left. \frac{\partial \bar{F}}{\partial \bar{t}} \right|_{\bar{x}_0} = \frac{\partial \bar{F}}{\partial \bar{t}} + \frac{\partial \bar{F}}{\partial \bar{X}} \frac{\partial \bar{X}}{\partial \bar{t}} = \frac{\partial \bar{F}}{\partial \bar{t}} + \frac{\partial \bar{F}}{\partial \bar{X}} \bar{W}. \tag{13}$$

Similarly, after using Eq. (3), Eq. (13) reduces to

$$\bar{W} = \frac{-\frac{Cl_{ks}}{\omega} \left\{ \bar{\beta}_1 \bar{\epsilon}_1 \cos\left(\frac{\bar{\beta}_1}{\omega}(\bar{X} - s\bar{t})\right) + \bar{\beta}_2 \bar{\epsilon}_2 \cos\left(\frac{\bar{\beta}_2}{\omega}(\bar{X} - s\bar{t})\right) + \bar{\beta}_3 \bar{\epsilon}_3 \cos\left(\frac{\bar{\beta}_3}{\omega}(\bar{X} - s\bar{t})\right) \right\}}{1 - \frac{Cl_k}{\omega} \left\{ \bar{\beta}_1 \bar{\epsilon}_1 \cos\left(\frac{\bar{\beta}_1}{\omega}(\bar{X} - s\bar{t})\right) + \bar{\beta}_2 \bar{\epsilon}_2 \cos\left(\frac{\bar{\beta}_2}{\omega}(\bar{X} - s\bar{t})\right) + \bar{\beta}_3 \bar{\epsilon}_3 \cos\left(\frac{\bar{\beta}_3}{\omega}(\bar{X} - s\bar{t})\right) \right\}}. \tag{14}$$

The above system of equations is expressed in an unsteady state and transforms this flow system from unsteady (time dependent) to steady (time independent) state by introducing the following mathematical relations which are defined as:

$$\begin{aligned} x' &= \bar{X} - s\bar{t}, \quad \xi' = \bar{\xi}, \quad w'(x', \xi') = \bar{W}(\bar{X}, \bar{\xi}, \bar{t}) - s, \quad u'(x', \xi') = \bar{U}(\bar{X}, \bar{\xi}, \bar{t}), \\ p'(x', \xi') &= \bar{P}(\bar{X}, \bar{\xi}, \bar{t}), \quad T'(x', \xi') = \bar{T}(\bar{X}, \bar{\xi}, \bar{t}) \end{aligned} \tag{15}$$

An analytical solution of the above system of equations is tractable by introducing the following non-dimensional parameters: $x = x'/\omega$, x is the axial coordinate, $\xi = \xi'/b$, ξ is the transverse coordinate, $t = s\bar{t}/\omega$, t is the time, $w = w'/s$, w is the axial velocity, $u = u'/\delta s$, u is the transverse velocity, $\delta = b/\omega$, δ is the wave number, $h = \bar{H}/b$, h is the upper wall, $\epsilon_i = \bar{C}_i/b$, ϵ_i represent the distinct amplitude ratios, $p = \bar{p}b^2/\mu\omega$, p is the pressure, $\alpha = \omega\bar{\alpha}/b$, α is the dimensionless divergent parameter, $\theta = (\bar{T} - T')/T'$, θ is the dimensionless temperature, $\gamma = (\bar{C} - C')/C'$, γ is the dimensionless species concentration, $\Omega = (\bar{\Omega} - \Omega')/\Omega'$, Ω is the dimensionless volume fraction of nanoparticle, $Re = \rho s b/\mu$, Re is the Reynolds number, $Pr = \mu(\rho c_p)/\rho_F k'$, Pr is the Prandtl number, $Q = \bar{Q}/sb$, Q is the dimensionless volumetric flow rate, $Grt = g\rho' a_i b^2 T'(1 - \Omega')/\mu s$, Grt is the thermal Grashof number, $Grc = g\rho' a_c b^2 C'(1 - \Omega')/\mu s$, Grc is the solutal Grashof number, $Grf = gb^2 \Omega'(\rho_p - \rho')/\mu s$, Grf is the nanoparticle Grashof number, $mt = dt(\rho c_p)_p/k'$, mt is the thermophoresis parameter, $mb = db(\rho c_p)_p \Omega'/k'$, mb is the Brownian motion parameter,

$\beta_i = s\bar{\beta}_i/\omega$, β_i ($i = 1 - 3$) are the distinct amplitude ratios, $Ha = B_0\sqrt{\sigma'/\rho}$, Ha is the Hartmann number (magnetic parameter), $Da = \sqrt{sK/\mu}$, Da is the Darcy's number (porosity parameter), $mct = dctT'/ds\zeta'$, mct is the Soret parameter, $mtc = dtc\zeta'/k'T'$, and mtc is the Dufour parameter.

For more simplification, the velocity components can also be express in the term of a stream function as:

$$w = \frac{\partial \psi}{\partial \xi}, \quad u = -\frac{\partial \psi}{\partial x}. \tag{16}$$

After using scaling variables, the dimensionless form of radial and axial components of velocity is:

$$u = \frac{-\alpha - Cl\{\beta_1 \in_1 \cos(\beta_1x) + \beta_2 \in_2 \cos(\beta_2x) + \beta_3 \in_3 \cos(\beta_3x)\}}{1 - \alpha - Cl\{\beta_1 \in_1 \cos(\beta_1x) + \beta_2 \in_2 \cos(\beta_2x) + \beta_3 \in_3 \cos(\beta_3x)\}}, \tag{17}$$

$$\text{and } w = \frac{-1}{1 - Cl\kappa\{\beta_1 \in_1 \cos(\beta_1x) + \beta_2 \in_2 \cos(\beta_2x) + \beta_3 \in_3 \cos(\beta_3x)\}}. \tag{18}$$

After using dimensionless variables, applying the long wavelength and the low Reynolds number approximations, the above system of equations reduces to

$$-\frac{dp}{dx} + \frac{\partial^2 w}{\partial \xi^2} - \left(\frac{Ha^2}{1 + M^2} + \frac{1}{Da^2} \right) (w + 1) + Grt\theta + Grc\gamma + Grf\Omega = 0, \tag{19}$$

$$\frac{dp}{d\xi} = 0, \tag{20}$$

$$\frac{\partial^2 \theta}{\partial \xi^2} + mtc \frac{\partial^2 \gamma}{\partial \xi^2} + mb \frac{\partial \Omega}{\partial \xi} \frac{\partial \theta}{\partial \xi} + mt \left(\frac{\partial \theta}{\partial \xi} \right)^2 = 0, \tag{21}$$

$$\frac{\partial^2 \gamma}{\partial \xi^2} + mct \frac{\partial^2 \theta}{\partial \xi^2} = 0, \tag{22}$$

$$\frac{\partial^2 \Omega}{\partial \xi^2} + \frac{mt}{mb} \frac{\partial^2 \theta}{\partial \xi^2} = 0, \tag{23}$$

$$\text{Let, } R^2 = \frac{Ha^2}{1 + M^2} + \frac{1}{Da^2}.$$

The alternative form of Eq. (19) is obtained by applying the cross-derivative between Eqs. (19) and (20). Then, Eq. (19) will reduce to:

$$\frac{\partial}{\partial \xi} \left(\frac{\partial^2 w}{\partial \xi^2} - R^2(w + 1) + Grt\theta + Grc\gamma + Grf\Omega \right) = 0, \tag{24}$$

$$\frac{\partial^3 w}{\partial \xi^3} - R^2 \frac{\partial w}{\partial \xi} + Grt \frac{\partial \theta}{\partial \xi} + Grc \frac{\partial \gamma}{\partial \xi} + Grf \frac{\partial \Omega}{\partial \xi} = 0 \tag{25}$$

The boundary and thermal conditions for the present flow model are prescribed as:

$$\frac{\partial w}{\partial \xi} = 0, \quad \theta = 0, \quad \gamma = 0, \quad \Omega = 0, \quad \text{at } \xi = 0, \tag{26}$$

$$w = \frac{-1}{1 - Cl\kappa\{\beta_1 \in_1 \cos(\beta_1x) + \beta_2 \in_2 \cos(\beta_2x) + \beta_3 \in_3 \cos(\beta_3x)\}}, \quad \theta = 1, \quad \gamma = 1, \quad \Omega = 1, \quad \text{at } \xi = h(x) = Cl(\varepsilon_1 \sin(\beta_1x) + \varepsilon_2 \sin(\beta_2x) + \varepsilon_3 \sin(\beta_3x)) + 1 + \alpha x, \tag{27}$$

2.2 Exact solutions

The exact solution of the heat phenomena is obtained after simplification that is given below:

$$\theta = A_{11} \frac{e^{-\zeta \xi}}{\zeta} + A_{12}, \tag{28}$$

where A_{11} and A_{12} are integration constants. Their values are obtained by using appropriate boundary conditions (26b) and (27b):

$$A_{11} = -\frac{e^{h\zeta} \zeta}{-1 + e^{h\zeta}} \text{ and } A_{12} = \frac{e^{h\zeta}}{-1 + e^{h\zeta}},$$

where $\zeta = \frac{1}{h} \left(\frac{mt+mb}{1-mctmtc} \right)$.

The exact solution of the concentration equation is

$$\gamma = -\frac{mt}{mb} \frac{\partial \theta}{\partial \xi} + \frac{1}{h} \left(1 + \frac{mt}{mb} \right) \xi. \tag{29}$$

For more simplification, Eq. (29) can also be expressed as after applying derivative with respect to ξ to Eq. (28) and putting in Eq. (29), we acquire

$$\gamma = A_{11} \frac{mt}{mb} \frac{e^{-\zeta \xi}}{\zeta^2} + \frac{1}{h} \left(1 + \frac{mt}{mb} \right) \xi. \tag{30}$$

The exact solution of the volumetric fraction of nanoparticles is

$$\Omega = -mct \frac{\partial \theta}{\partial \xi} + \frac{1}{h} (1 + mct) \xi. \tag{31}$$

Alternative form of Eq. (31) is obtained after substituting Eq. (28) in Eq. (31), we acquire

$$\Omega = A_{11} mct \frac{e^{-\zeta \xi}}{\zeta^2} + \frac{1}{h} (1 + mct) \xi. \tag{32}$$

Exact solution of the axial velocity is obtained by using appropriate boundary conditions given in Eqs. (26a) and (27a) with the help of **Mathematica 10.0 Software**.

$$\begin{aligned} w = & \left\{ e^{-h(R+\zeta)-\xi(2R+\zeta)} \left(e^{(h+\zeta)(R+\zeta)} hGrcmb(1+mct) \left(e^{2hR} - e^{2R\zeta} - e^{hR} hR - e^{(h+2\zeta)R} hR \right. \right. \right. \\ & + e^{R\zeta} R\zeta + e^{R(2h+\zeta)} R\zeta \alpha \left(R^2 - \alpha^2 \right) + \left. \left. \left(A_{11} e^{(h+\zeta)R} hBR \left(e^{R\xi+h\alpha} R + e^{2hR+R\zeta+h\alpha} R - e^{Rh+\alpha\xi} R \right. \right. \right. \right. \\ & - e^{hR+2R\zeta+h\alpha} R - e^{2hR+h\alpha+\zeta\alpha} \alpha + e^{2R\zeta+h\alpha+\zeta\alpha} \alpha \left. \right) + \left(e^{\zeta(R+\alpha)+h(3R+\alpha)} \text{Grf}(mb+mt) \right. \\ & - e^{\zeta(R+\alpha)+\xi(3R+\alpha)} \text{Grf}(mb+mt) + e^{3hR+2R\xi+h\alpha+\xi\alpha} R \left(A_{12} hB - hmbPx + \text{Grf}(mb+mt)\xi \right) \\ & + e^{hR+2R\xi+h\alpha+\xi\alpha} hR \left(A_{12} hB - hmbPx + \text{Grf}(mb+mt)\xi \right) + e^{2hR+3R\xi+h\alpha+\xi\alpha} hR \\ & \left. \left. \left. - \text{Grf}(mb+mt - A_{12}mt) + mb \left(-A_{12}Grt + A_{12}Grmct + Px + R^2z \right) \right\} / \right. \\ & \left. \left(\left(1 + e^{2hR} \right) hmbR^3 \alpha \left(R^4 - \alpha^2 \right) h \right). \tag{33} \right. \end{aligned}$$

The mathematical form of the pressure gradient is acquired by putting Eqs. (28), (30), (32) and (33) in Eq. (19):

$$\begin{aligned}
\frac{dp}{dx} = & - \left\{ 2e^{h(R+\zeta)} h \text{Gr} \text{cmb} (1 + \text{mb}) \zeta^2 (R^2 - \zeta^2) - e^{h(R+\zeta)} h \text{Gr} \text{cmb} (1 + \text{mct}) (2 + h^2 R) \zeta^2 \right. \\
& (R^2 - \zeta^2) \cosh[hR] + 2e^{h(R+\zeta)} h \text{Gr} \text{f} (\text{mb} + \text{mt}) \zeta^2 (R^2 - \zeta^2) + A_{11} B h R \left((-1 + e^{2hR}) \right. \\
& \left. (-1 + e^{h\zeta}) R^2 + (-1 + e^{2hR}) R \zeta + e^{h\zeta} (-1 + e^{hR})^2 \zeta^2 \right) h - 2A_{12} B e^{h(R+\zeta)} h^3 R^2 \zeta^2 (R^2 - \zeta^2) \cos h[hR] \\
& + 2e^{h(R+\zeta)} h^2 \text{mb} Q R^4 \zeta^2 (R^2 - \zeta^2) \cos h[hR] - 2e^{h(R+\zeta)} h \text{Gr} \text{f} (\text{mb} + \text{mt}) (2 + h^2 R^2) \zeta^2 (R^2 - \zeta^2) \\
& \cos h[hR] + 2e^{h(R+\zeta)} h^2 \text{Gr} \text{c} (1 + \text{mct}) R \zeta^2 (R^2 - \zeta^2) \sin h[hR] + 2A_{12} e^{h(R+\zeta)} h^2 \text{Gr} \text{tmb} R \zeta^2 \\
& (R^2 - \zeta^2) \sin h[hR] - 2A_{12} e^{h(R+\zeta)} h^2 \text{Gr} \text{cmb} \text{mct} R \zeta^2 (R^2 - \zeta^2) \sin h[hR] + 2e^{h(R+\zeta)} h \text{Gr} \text{f} \\
& (\text{mb} + \text{mt} - A_{12} \text{mt}) R \zeta^2 (R^2 - \zeta^2) \sin h[hR] - 2e^{h(R+\zeta)} h^2 \text{mb} R^{3/2} \zeta^2 (R^2 - \zeta^2) \sin h[hR] \left. \right\} / \\
& \left(2e^{h(R+\zeta)} h^2 \text{mb} R^2 \zeta^2 (R^2 - \zeta^2) \cos h[hR] - 2e^{h(R+\zeta)} h^2 \text{mb} R \zeta^2 (R^2 - \zeta^2) \sin h[hR] \right). \quad (34)
\end{aligned}$$

3 Results and discussions

In this section, the physical effects of involved parameters on the flow features are analyzed with the help of graphs. The flow diagram of a non-uniform complex ciliated channel is displayed in Fig. 1. Representative results for the axial velocity profile, pressure gradient, nanoparticles volumetric fraction, heat and mass transfer phenomena are illustrated in Figs. 2, 3, 4, 5 and 6 below. These figures are plotted through **Mathematica Software 10.0**.

The physical influence of flow parameters on the velocity profile is displayed in Fig. 2. These graphs are plotted at four dissimilar cross sections, say $\chi = 0.1, 0.3, 0.6$ and 0.9 . Figure 2a displays the influence of thermophoresis parameter, mt , on the velocity profile. There is a strong increase in the magnitude of velocity, with a rise in mt value from 0 to 15 at cross sections $\chi = 0.3, 0.6$ and 0.9 , and reverse pattern is predicted at cross section $\chi = 0.1$. These outcomes are observed under Hall and porosity effects. Physically, this graph shows that the thermophoresis parameter, mt , has a sound impact on the augmentation of velocity magnitude. Figure 2b displays the influence of a divergent parameter, α , on the velocity profile. There is a strong increase in the magnitude of velocity near the center of the channel, say $\xi = 0$, and opposite trend is predicted near the boundary walls with a rise in α value from 0 to 0.15 at can cross-sections $\chi = 0.1, 0.3, 0.6$ and 0.9 . Additionally, these consequences are observed under Hall and porosity effects. Physically, this graph shows that the divergent parameter, α , has a dynamic impact on the augmentation of velocity magnitude near the center of the channel, say $\xi = 0$, and opposite trend is predicted near the boundary walls. Figure 2c illustrates the velocity profile response with an enhancement in cilia length parameter under thermophoresis, Hall and porosity effect. The magnitude of velocity profile is boosted by increase in the cilia length, Cl , from 0 to 0.15. Physically, this result shows that the larger numeric values of cilia length parameter overcome the physical effects of Hall and porosity parameters. The influence of Soret parameter, mct , on the velocity profile is displayed in Fig. 2d under Hall and porosity effects. The magnitude of velocity profile increases by increasing the numeric values of mct from 0 to 15. The obtained results are same in each cross section but enhancement in the magnitude of velocity profile at cross section $\chi = 0.9$ much larger than the other cross sections under Hall and porosity effects. Physically, this result shows that the presence of Soret effects is much larger than $\text{mct} = 0$ and cross-sectional area has a dynamic role in enhancement of velocity profile. The physical effects of Hall parameter on the velocity profile are shown in Fig. 2e under thermophoresis, magnetic and

porosity effects. Physically, these results show that the larger numeric values of Hall parameter overcome the influence of magnetic field and thermophoresis effects. Similar nature of results is predicted in each cross-sectional area. Figure 2f deals with the physical impacts of porosity

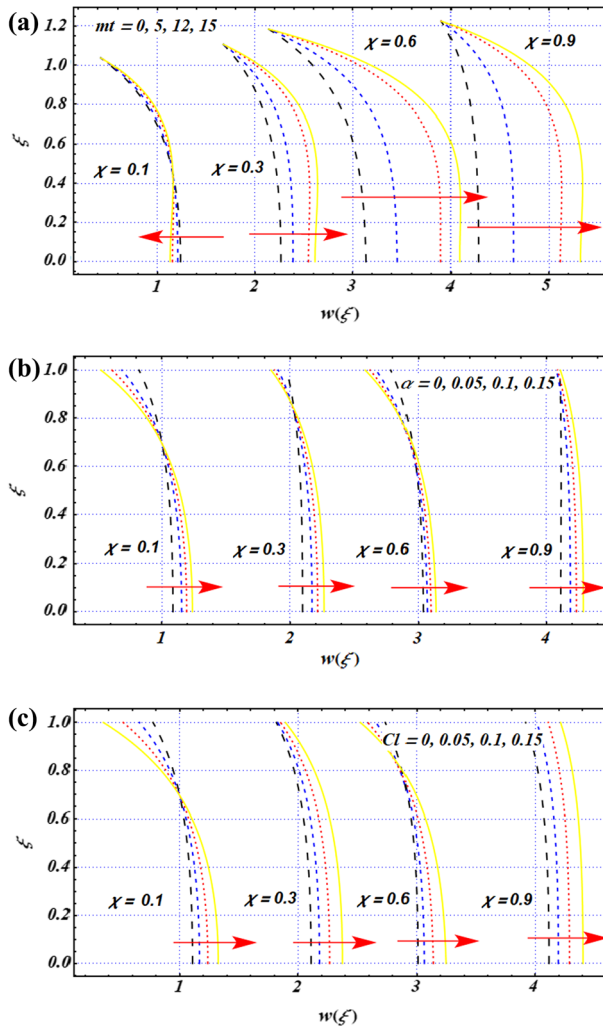


Fig. 2 Variation of mt on velocity profile at $\alpha = 0.2$, $mb = 0.2$, $mct = 0.1$, $mtc = 0.1$, $\beta_1 = 1$, $\beta_2 = 2$, $\beta_3 = 3$, $Ha = 2$, $M = 1$, $Da = 1$, $Gr_t = Gr_c = Gr_f = 0.1$, $\varepsilon_1 = 0.1$, $\varepsilon_2 = 0.2$, $\varepsilon_3 = 0.4$ **b** Variation of α on velocity profile at $mb = 0.2$, $mt = mct = mtc = 0.1$, $\beta_1 = 1$, $\beta_2 = 2$, $\beta_3 = 3$, $Ha = 2$, $M = 1$, $Da = 1$, $Gr_t = Gr_c = Gr_f = Cl = 0.1$, $k = 1$, $\varepsilon_1 = 0.1$, $\varepsilon_2 = 0.2$, $\varepsilon_3 = 0.4$. **c** Variation of Cl on velocity profile at $mb = 0.2$, $mt = mct = mtc = 0.1$, $\beta_1 = 1$, $\beta_2 = 2$, $\beta_3 = 3$, $Ha = 2$, $M = 1$, $Da = 1$, $Gr_t = Gr_c = Gr_f = \alpha = 0.1$, $k = 1$, $\varepsilon_1 = 0.1$, $\varepsilon_2 = 0.2$, $\varepsilon_3 = 0.4$. **d** Variation of mct on velocity profile at $mb = 0.2$, $Cl = mt = mtc = 0.1$, $\beta_1 = 1$, $\beta_2 = 2$, $\beta_3 = 3$, $Ha = 2$, $M = 1$, $Da = 1$, $Gr_t = Gr_c = Gr_f = \alpha = 0.1$, $k = 1$, $\varepsilon_1 = 0.1$, $\varepsilon_2 = 0.2$, $\varepsilon_3 = 0.4$. **e** Variation of M on velocity profile at $\alpha = 0.2$, $mb = 0.2$, $mt = mct = mtc = 0.1$, $\beta_1 = 1$, $\beta_2 = 2$, $\beta_3 = 3$, $Ha = 2$, $Da = 1$, $Gr_t = Gr_c = Gr_f = 0.1$, $\varepsilon_1 = 0.1$, $\varepsilon_2 = 0.2$, $\varepsilon_3 = 0.4$. **f** Variation of Da on velocity profile at $\alpha = 0.2$, $mb = 0.2$, $mt = mct = mtc = 0.1$, $\beta_1 = 1$, $\beta_2 = 2$, $\beta_3 = 3$, $Ha = 2$, $M = 1$, $Gr_t = Gr_c = Gr_f = 0.1$, $\varepsilon_1 = 0.1$, $\varepsilon_2 = 0.2$, $\varepsilon_3 = 0.4$

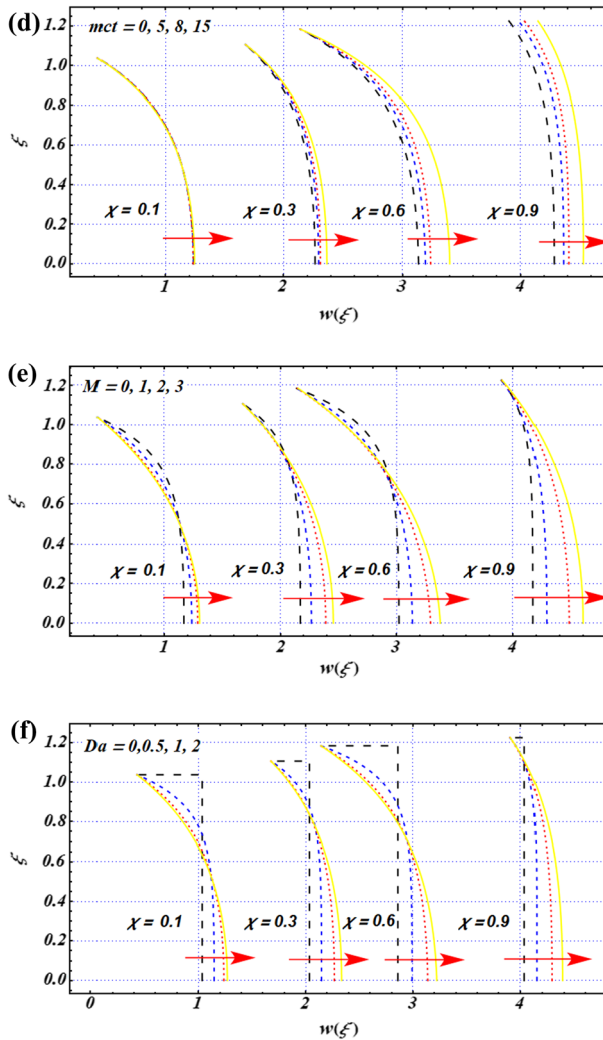


Fig. 2 continued

parameter on the velocity profile under Hall and thermophoresis effects. The magnitude of velocity profile is enhanced by increasing numeric value of porosity parameter under Hall effects. The boundary layer phenomena are obtained in the velocity profile at larger porosity effects. Physically, this result shows that the boundary layer phenomena in the velocity profile are obtained for smaller numeric values of porosity parameter, and larger numeric values of Darcy's number overcome the magnetic and thermophoresis effects. All these results are obtained for the complex wavy pattern of ciliated boundary walls.

In Fig. 3, the influence of various embedded parameters on the pressure gradient is depicted. These graphs are plotted for a complex wavy scenario of metachronal waves. Figure 3a deals with the influences of porosity parameter on the pressure gradient under Hall and thermophoresis effects. The magnitude of pressure gradient is reduced as numeric values of the porosity parameter enhance from 0.4 to 2. Additionally, wavy shape in the behavior of

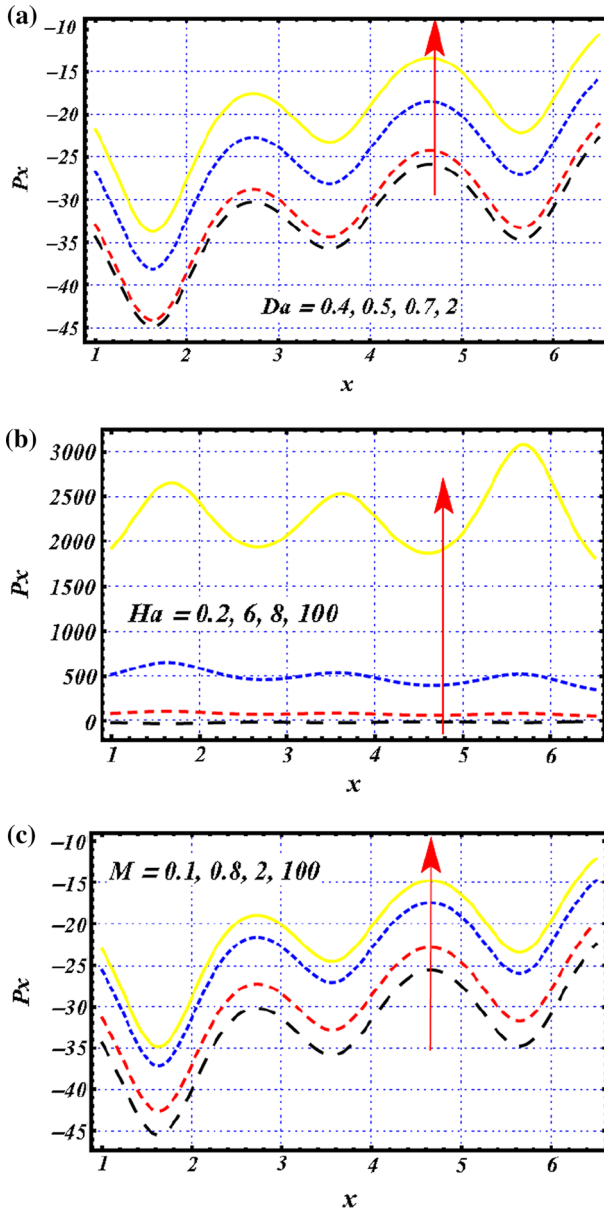


Fig. 3 **a** Variation of Da on pressure gradient at $\alpha = 0.1, Ha = 0.5, M = 1, mb = mt = mct = mtc = 0.1, Grt = Grf = Grc = 0.1, Cl = 0.5, k = 1, \beta_1 = 1, \beta_2 = 2, \beta_3 = 3, \epsilon_1 = 0.1, \epsilon_2 = 0.2, \epsilon_3 = 0.4$ **b** Variation of Ha on pressure gradient at $\alpha = 0.1, Da = 3, M = 1, mb = mt = mct = mtc = 0.1, Grt = Grf = Grc = 0.1, Cl = 0.5, k = 1, \beta_1 = 1, \beta_2 = 2, \beta_3 = 3, \epsilon_1 = 0.1, \epsilon_2 = 0.2, \epsilon_3 = 0.4$. **c** Variation of M on pressure gradient at $\alpha = 0.1, Da = 3, Ha = 1, mb = mt = mct = mtc = 0.1, Grt = Grf = Grc = 0.1, Cl = 0.5, k = 1, \beta_1 = 1, \beta_2 = 2, \beta_3 = 3, \epsilon_1 = 0.1, \epsilon_2 = 0.2, \epsilon_3 = 0.4$. **d** Variation of Grt on pressure gradient at $\alpha = 0.1, Ha = 1, Da = 3, M = 1, mb = mt = mct = mtc = 0.1, Grf = Grc = 0.1, Cl = 0.5, k = 1, \beta_1 = 1, \beta_2 = 2, \beta_3 = 3, \epsilon_1 = 0.1, \epsilon_2 = 0.2, \epsilon_3 = 0.4$. **e** Variation of Grf on pressure gradient at $\alpha = 0.1, Ha = 1, Da = 3, M = 1, mb = mt = mct = mtc = 0.1, Grt = Grc = 0.1, Cl = 0.5, k = 1, \beta_1 = 1, \beta_2 = 2, \beta_3 = 3, \epsilon_1 = 0.1, \epsilon_2 = 0.2, \epsilon_3 = 0.4$

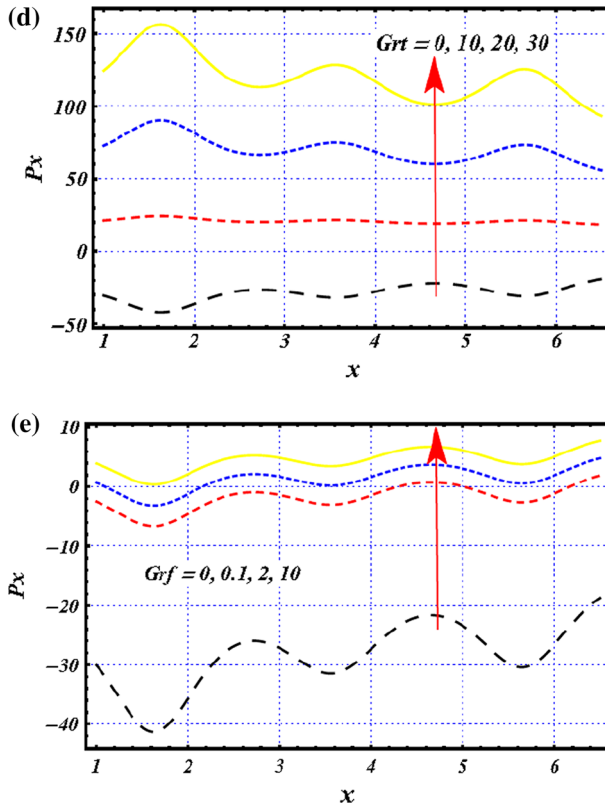


Fig. 3 continued

pressure gradient is easily observed due to the wavy nature of metachronal waves. Physically, these results show that under larger porosity effects, the magnitude of pressure gradient is larger via compared with smaller strength of porosity effect. The influence of magnetic field on the pressure gradient is displayed in Fig. 3b under Hall and thermophoresis effects. It is predicted that for the smaller strength of magnetic field, the magnitude of pressure gradient is smaller in magnitude via compared with the larger strength of magnetic field. Physically, it shows that as the numeric values of magnetic parameter increase, the magnitude of pressure gradient is boosted too. In other words, it can say that the magnetic field has a dynamic role in enhancement of the pressure gradient under thermophoresis, Hall and porosity effects. In Fig. 3c, the pressure gradient with variation of x for various values of Hall parameter is displayed. These results are achieved under larger magnetic and porosity effects. The magnitude of pressure gradient is reduced by increasing the numeric value of Hall parameter from 0.1 to 100. Physically, the larger strength of Hall parameter overcomes the magnetic and thermophoresis effect. In other word, the magnitude of pressure gradient is larger for smaller numeric values of Hall parameter as compared with the larger strength of Hall device effects. Figure 3d deals with the impacts of thermal Grashof number on the pressure gradient under Hall and porosity effects. The magnitude of pressure gradient is sharply enhanced via increasing the numeric value of Gr_t from 0 to 30. In the absence of Gr_t , the physical effect of porosity and Hall parameters are dominant when compared with the presence of thermal Grashof number. The physical impacts of nanoparticle Grashof number are displayed

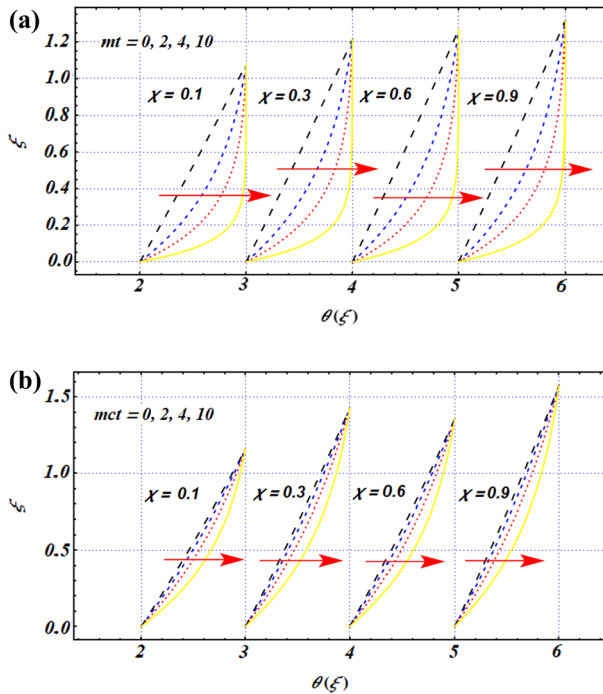


Fig. 4 a Variation of mt on heat transfer at $\alpha = 0.1$, $mb = mct = mtc = 0.1$, $Gr_t = Gr_f = Gr_c = 0.1$, $Cl = 0.4$, $k = 1$, $\beta_1 = 1$, $\beta_2 = 2$, $\beta_3 = 3$, $\varepsilon_1 = 0.1$, $\varepsilon_2 = 0.2$, & $\varepsilon_3 = 0.4$ **b** Variation of mct on heat transfer at $\alpha = 0.1$, $mt = mb = mtc = 0.1$, $Gr_t = Gr_f = Gr_c = 0.1$, $Cl = 0.4$, $k = 1$, $\beta_1 = 1$, $\beta_2 = 2$, $\beta_3 = 3$, $\varepsilon_1 = 0.1$, $\varepsilon_2 = 0.2$, & $\varepsilon_3 = 0.4$

in Fig. 3e under Hall and porosity effects. In the absence of Gr_f , the magnitude of pressure gradient has larger in magnitude via compared with the nonzero numeric values of Gr_f .

Figure 4 deals with the influence of thermophoresis and Soret parameters on the heat transfer concerned with the ciliated transportation of nanofluid along with double diffusion convection through a complex divergent channel. These diagrams are plotted at four different cross sections, say $\chi = 0.1, 0.3, 0.6, 0.9$. It is obvious through Fig. 4a, the magnitude of heat transfer phenomena is augmented by enhancing the numeric value of the thermophoresis parameter from 0 to 10. Physically, it means that the magnitude of heat transfer for nonzero numeric values of thermophoresis parameter is much larger than $mt = 0$. Similarly, the magnitude of heat transfer phenomena is increased by the numeric values of Soret parameter from 0 to 9 under thermophoresis influences (see in Fig. 4b). Physically, these results show that the magnitude of heat transfer in the presence of Soret influences is much larger than $mct = 0$.

Figure 5 deals with the influence of thermophoresis and Soret parameters on the mass concentration concerned with the ciliated transportation of nanofluid along with double diffusion convection through a complex divergent channel. These diagrams are plotted at four different cross sections, say $\chi = 0.1, 0.3, 0.6, 0.9$. It is obvious through Fig. 5a, the magnitude of mass concentration is augmented by enhancing the numeric value of the thermophoresis parameter from 0 to 50. Physically, it means that the magnitude of mass concentration for nonzero numeric values of thermophoresis parameter is much larger than $mt = 0$. Similarly,

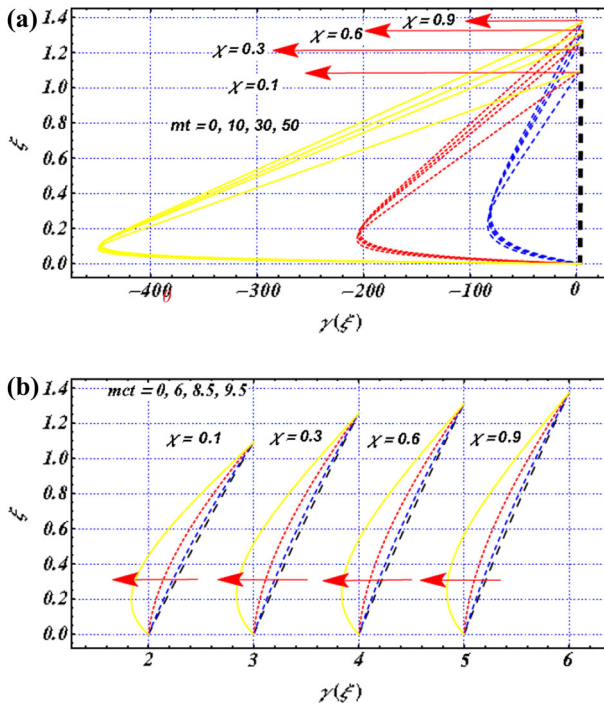


Fig. 5 a Variation of mt on mass concentration at $\alpha = 0.1$, $mct = mb = mtc = 0.1$, $Gr_t = Gr_f = Gr_c = 0.1$, $Cl = 0.4$, $k = 1$, $\beta_1 = 1$, $\beta_2 = 2$, $\beta_3 = 3$, $\varepsilon_1 = 0.1$, $\varepsilon_2 = 0.2$, & $\varepsilon_3 = 0.4$. **b** Variation of mct on mass concentration at $\alpha = 0.1$, $mt = mb = mtc = 0.1$, $Gr_t = Gr_f = Gr_c = 0.1$, $Cl = 0.4$, $k = 1$, $\beta_1 = 1$, $\beta_2 = 2$, $\beta_3 = 3$, $\varepsilon_1 = 0.1$, $\varepsilon_2 = 0.2$, & $\varepsilon_3 = 0.4$

the magnitude of mass concentration is increased by the numeric values of Soret parameter from 0 to 9.5 under thermophoresis influences (see in Fig. 5b). Physically, these results show that the magnitude of mass concentration in the presence of Soret influences is much larger than $mct = 0$.

Figure 6 deals with the influence of thermophoresis and Soret parameters on the nanoparticle volumetric fraction concerned with the ciliated transportation of nanofluid along with double diffusion convection through a complex divergent channel. These diagrams are plotted at four different cross sections, say $\chi = 0.1, 0.3, 0.6, 0.9$. It is obvious through Fig. 6(a), the magnitude of nanoparticle volumetric fraction is augmented by enhancing the numeric value of the thermophoresis parameter from 0 to 100. Physically, it means that the magnitude of nanoparticle volumetric fraction for nonzero numeric values of thermophoresis parameter is much larger than $mt = 0$. Similarly, the magnitude of nanoparticle volumetric fraction is increased by the numeric values of Soret parameter from 0 to 9.5 under thermophoresis influences (see in Fig. 6b). Physically, these results show that the magnitude of nanoparticle volumetric fraction in the presence of Soret influences is much larger than $mct = 0$.

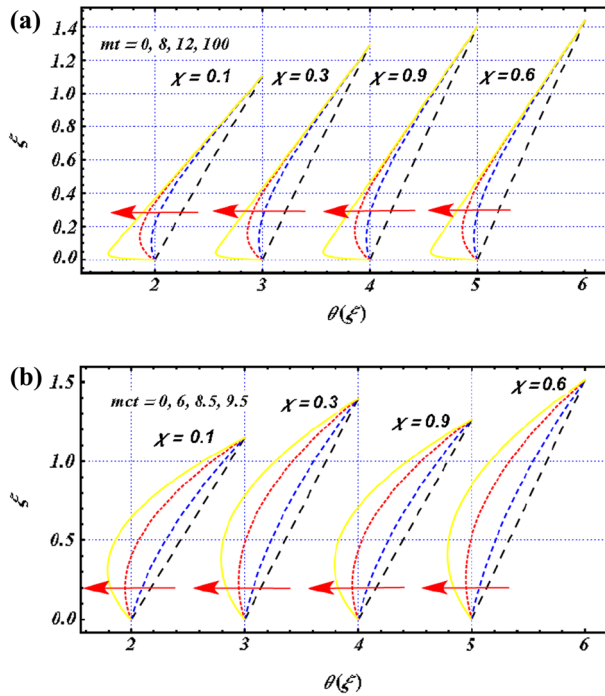


Fig. 6 a Variation of mt on nanoparticle volumetric fraction at $\alpha = 0.1$, $mct = mb = mtc = 0.1$, $Gr_t = Gr_f = Gr_c = 0.1$, $Cl = 0.4$, $k = 1$, $\beta_1 = 1$, $\beta_2 = 2$, $\beta_3 = 3$, $\varepsilon_1 = 0.1$, $\varepsilon_2 = 0.2$, $\varepsilon_3 = 0.4$
b Variation of mct on nanoparticle volumetric fraction at $\alpha = 0.1$, $mt = mb = mtc = 0.1$, $Gr_t = Gr_f = Gr_c = 0.1$, $Cl = 0.4$, $k = 1$, $\beta_1 = 1$, $\beta_2 = 2$, $\beta_3 = 3$, $\varepsilon_1 = 0.1$, $\varepsilon_2 = 0.2$, $\varepsilon_3 = 0.4$

4 Conclusions

A mathematical problem has been presented for the creeping ciliated flow from a non-uniform channel in the presence of double diffusion convection, Hall and porosity effects. The obtained governing equations have been non-dimensionalized using similarity transformations. The solution of the flow problem is obtained by using an integration method. Graphs of flow features are plotted through Mathematica software 10.0 for the complex metachronal waves. The physical impact of involved parameters on the flow features has been presented graphically and discussed in detail. A few dynamic flow characteristics have been determined, and these are summarized as follows:

- The non-uniform and cilia length parameters have a dynamic role in enhancement of velocity profile. By increasing the numerical values of thermophoresis and Soret parameters, the magnitude of velocity profile is also enhanced under Hall and porous medium. Hall device has sound effects on the augmentation of velocity profile under porosity effects. All these physical influences on the velocity profile are noticed at four different cross sections in a wave frame. The boundary layer in the velocity profile is obtained under larger magnetic and porosity effects.
- The pressure gradient is reduced for larger porosity effect and reverse trend is noticed for larger strength of magnetic effects. Hall device and thermal Grashof number have dynamic

roles in enhancement of pressure gradient. Due to the complex nature of ciliated wall, the wavy pattern is present in the pressure gradient.

- The thermal Grashof number and solutal Grashof number have a sound impact in enhancement of heat transfer phenomena and nanoparticle volumetric fraction for ciliated flow of nanofluid.
- The solutal Grashof number boosts the magnitude of mass concentration of nanofluid.
- The complex wavy pattern is obtained for fixed value of amplitude ratios, say as $\varepsilon_1 = 0.1$, $\varepsilon_2 = 0.2$, & $\varepsilon_3 = 0.4$.
- The graphs of velocity profile, heat transfer, mass transfer and volumetric fraction are plotted at four distinct cross sections in wave frame.

Acknowledgements The authors extend their appreciation to the Deanship of Scientific Research at King Khalid University, Abha 61413, Saudi Arabia, for funding this work through research groups program under grant number R.G.P-1/234/42.

Funding There is no funding for this submission.

Declarations

Conflict of interest The authors declare that there are no conflicts of interests with publication of this work.

Ethical standards The authors ensure the compliance with ethical standards for this work.

References

1. J.R. Blake, Flow in tubules due to ciliary activity. *Bull. Math. Biol.* **35**, 513–523 (1973)
2. J.R. Blake, M.A. Sleight, Mechanics of Ciliary Locomotion. *Biol. Rev.* **49**, 85–125 (1974)
3. N. Liron, S. Mochon, Stokes flow for a stokeslet between two parallel flat plates. *J. Eng. Math.* **10**, 287 (1976)
4. M.A. Sleight, *The Biology of Cilia and Flagella* (MacMillan, New York, 1962)
5. H. Agarwal, Anwaruddin, , Cilia transport of biofluid with variable viscosity. *Indian J. Pure Appl. Math.* **15**, 1128–1139 (1984)
6. I. Ibanez-Tallon, N. Heintz, H. Omran, To beat or not to beat: role of cilia in development and disease. *Hum. Mol. Genet.* **12**, 27–35 (2003)
7. J. Hussong, W.-P. Breugem, J. Westerweel, A continuum model for flow induced by metachronal coordination between beating cilia. *J. Fluid Mech.* **684**, 137–162 (2011)
8. R.R. Velez-Cardero, E. Lauga, Waving transport and propulsion in a generalized Newtonian fluid. *J. Non-Newtonian Fluid Mech.* **199**, 37–50 (2013)
9. A. Dauplain, J. Favier, A. Bottaro, Hydrodynamics of ciliary propulsion. *J. Fluids Struct.* **24**, 1156–1165 (2008)
10. A.M. Siddiqui, A.A. Farooq, M.A. Rana, Study of MHD effects on the cilia-induced flow of a Newtonian fluid through a cylindrical tube. *Magneto hydrodynamics* **50**(4), 249–261 (2014)
11. A.M. Siddiqui, A.A. Farooq, M.A. Rana, Hydromagnetic flow of Newtonian fluid due to ciliary motion in a channel. *Magneto hydrodynamics* **50**(3), 109–122 (2014)
12. A. Ahmad Farooq, Z. Shah, E.O. Alzahrani, Heat transfer analysis of a magneto-bio-fluid transport with variable thermal viscosity through a vertical ciliated channel. *Symmetry* **11**(10), 1240 (2019)
13. Z. Asghar, K. Javid, M. Waqas, A. Ghaffari, W.A. Khan, Cilia-driven fluid flow in a curved channel: effects of complex wave and porous medium. *Fluid Dyn. Res.* **52**(1), 015514 (2020)
14. K. Javid, M. Riaz, Y.M. Chu, M.I. Khan, S.U. Khan, S. Kadry, Peristaltic activity for Electro-kinetic complex driven cilia transportation through a non-uniform channel. *Comput. Methods Progr. Biomed.* **200**, 105926 (2021)

15. S. U. S. Choi, Enhancing thermal conductivity of fluids with nanoparticles, in *Proceedings of the ASME International Mechanical Engineering Congress and Exposition, ASME, FED 231/MD*, 66, p. 99, San Francisco, Calif, USA (1995)
16. O.D. Makinde, A. Aziz, Boundary layer flow of a nanofluid past a stretching sheet with a convective boundary condition. *Int. J. Therm. Sci.* **50**(7), 1326–1332 (2011)
17. E.H. Aly, A. Ebaid, N.Y. Abdelazem, Analytical and numerical investigations for the flow and heat transfer of nanofluids over a stretching sheet with partial slip boundary condition. *Appl. Math. Inf. Sci.* **8**(4), 1639–1645 (2014)
18. S. Das, B. Tarafdar, R.N. Jana, O.D. Makinde, Influence of wall conductivities on a fully developed mixed-convection magnetohydrodynamic nanofluid flow in a vertical channel. *J. Eng. Phys. Thermophys.* **91**(3), 784–796 (2018)
19. S. Shaheen, K. Maqbool, A.M. Siddiqui, Micro rheology of Jeffrey nanofluid through cilia beating subject to the surrounding temperature. *RheologicaActa* **59**(8), 565–573 (2020)
20. A. Imran, R. Akhtar, Z. Zhiyu, M. Shoab, M.A.Z. Raja, Heat transfer analysis of biological nanofluid flow through ductus efferentes. *AIP Adv.* **10**(3), 035029 (2020)
21. A.V. Kuznetsov, D.A. Nield, Natural convective boundary-layer flow of a nanofluid past a vertical plate. *Int. J. Therm. Sci.* **49**(2), 243–247 (2010)
22. A.V. Kuznetsov, D.A. Nield, Double-diffusive natural convective boundary-layer flow of a nanofluid past a vertical plate. *Int. J. Therm. Sci.* **50**(5), 712–717 (2011)
23. O.A. Bég, D. Tripathi, Mathematica simulation of peristaltic pumping with double-diffusive convection in nanofluids: a bio-nano-engineering model. *Proc. Inst. Mech. Eng. Part N J. Nanoeng. Nanosyst.* **225**(3), 99–114 (2011)
24. D.A. Nield, A.V. Kuznetsov, The onset of double-diffusive convection in a nanofluid layer. *Int. J. Heat Fluid Flow* **32**(4), 771–776 (2011)
25. T. Hayat, S. Qayyum, S.A. Shehzad, A. Alsaedi, Cattaneo-Christov double-diffusion theory for three-dimensional flow of viscoelastic nanofluid with the effect of heat generation/absorption. *Res. Phys.* **8**, 489–495 (2018)
26. I.I. Ryzhkov, A.V. Minakov, The effect of nanoparticle diffusion and thermophoresis on convective heat transfer of nanofluid in a circular tube. *Int. J. Heat Mass Transf.* **77**, 956–969 (2014)
27. H. Alolaiyan, A. Riaz, A. Razaq, N. Saleem, A. Zeeshan, M.M. Bhatti, Effects of double diffusion convection on third grade nanofluid through a curved compliant peristaltic channel. *Coatings* **10**(2), 154 (2020)
28. H. Ge-JiLe, K. Javid, S. U. Khan, M. Raza, M. Ijaz Khan, S. Qayyum, Double diffusive convection and Hall effect in creeping flow of viscous nanofluid through a convergent microchannel: a biotechnological applications. *Comput. Methods Biomech. Biomed. Eng.*, pp. 1–18 (2021)